Observation of a Burstein–Moss Shift in Rhenium-Doped MoS_2 Nanoparticles

Qi -C. Sun,[⊥,†] Lena Yadgarov,[‡] Rita Rosentsveig,[‡] Gotthard Seifert,[§] Reshef Tenne,[‡] and Janice L. Musfeldt*[,†]

[†]Department of Chemistry, University of Tennessee, Knoxville, Tennessee 37996, United States , [‡]Department of Materials and Interfaces, Weizmann Institute of Science, RehoVot 76100, Israel, and [§]Physikalische Chemie, Technische Universität, 01062 Dresden, Germany. [⊥]Present address: Department of Chemical and Biological Engineering, University of Colorado, Boulder, Colorado 80309, United States.

ABSTRACT We investigated the optical properties of rhenium-doped MoS_2 nanoparticles and compared our findings with the pristine and bulk analogues. Our measurements reveal that confinement softens the exciton positions and reduces spin–orbit coupling, whereas doping has the opposite effect. We model the carrier-induced exciton blue shift in terms of the Burstein–Moss effect. These findings are important for understanding doping and finite length scale effects in low-dimensional nanoscale materials.

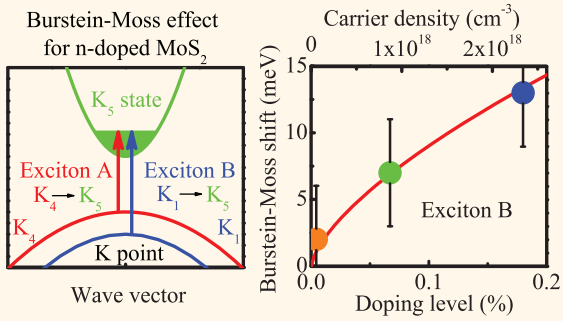

KEYWORDS: chalcogenides · nanoparticles · Burstein–Moss effect · spin–orbit coupling · optical conductivity

The Burstein–Moss shift was discovered independently by Burstein and Moss while researching the optical properties of InSb.[1,2] The effect arises from the Pauli exclusion principle and describes how adding electrons or holes to traditional semiconductors like CdSe, ZnO, and InGaAs controls carrier concentration, modifies the band gap, and enables control over the electronic structure.[3−8] Fundamental understanding of the optical response of these and other conventional semiconductors was thus partially responsible for the development of various electronic devices including photoelectrochemical cells, resonant-tunneling devices, Bragg mirrors, and surface-emitting lasers.[3−8] Layered transition metal dichalcogenides like the hexagonal molybdenum disulfide (2H-MoS_2, Figure 1a)[9,10] are also candidates for the investigation of Burstein–Moss effects, although early studies in which Re was used as the dopant did not display the classic signatures.[11−13] More recently, nanoscale analogues attracted attention, revealing ambipolar transistor behavior, superconductivity under gating, self-assembly, and photovoltaic character in nanocomposites, and enhanced tribological properties.[14−19] Rhenium-doped inorganic fullerene-like (IF) MoS_2 nanoparticles (herein abbreviated Re:IF-MoS_2)[20−23] provide an ideal physical platform for the investigation of n-doping effects in a confined system. In these systems, the Re centers act as substitutional dopants rather than interstitial impurities (Figure 1b).[22] Moreover, tunability with strain and electric field suggest that such a systematic exploration will prove useful.[24] There is an especially pressing need to connect the actual dopant concentration to the number of carriers in Re:IF-MoS_2. This is an enormously important issue for conventional bulk semiconductors[1,2] and quantum dots,[25] and the Burstein–Moss model provides a framework under which a quantitative relationship can be established. What differentiates our work from prior efforts is the two-dimensional nature of MoS_2 and the fact that the confined electrons do not have a well-defined periodicity.

Herein, we report the discovery of a Burstein–Moss effect in a nanoscale transition metal dichalcogenide (Figure 1c,d). Our measurements reveal that small size softens the exciton positions and reduces spin–orbit coupling, whereas doping has the opposite effect. On the basis of exciton and oscillator strength trends, we extract doping-induced

* Address correspondence to musfeldt@utk.edu.

Received for review January 28, 2013 and accepted March 11, 2013.

Published online March 11, 2013
10.1021/nn400464g

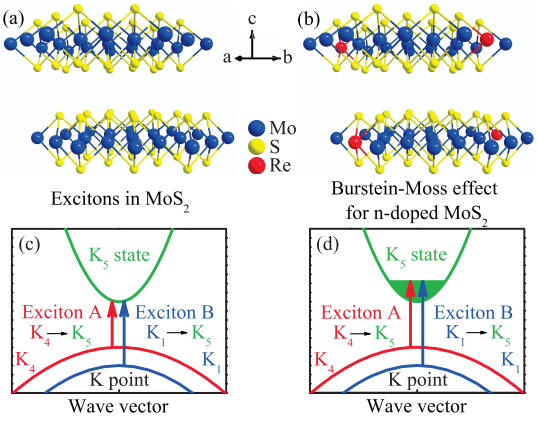

Figure 1. (a,b) Schematic views of the characteristic MoS_2 double layers along with an example of how the Re centers go into the lattice as substitutional impurities (rather than interstitial impurities), introduce extra electrons, and n-doped the material.[22] (c) Schematic view of the transitions corresponding to excitons A and B in pristine 2H- and IF-MoS_2. (d) Schematic view of the Burstein–Moss effect in electron doped MoS_2. In this work, we investigate Re-doped: IF-MoS_2. In both panels, excitons A and B are associated with optically allowed $K_4 \rightarrow K_5$ and $K_1 \rightarrow K_5$ transitions. Labels are according to refs 33 and 34.

changes in spin–orbit coupling and demonstrate that the carriers are bound rather than free. Taken together, these findings establish the relevance of the Burstein–Moss model[1−4,7,8] to metal dichalcogenide nanomaterials, extend the relationship between nominal and actual Re concentration[22] to include a quantitative connection to carrier density, and highlight the unique electronic character of Re:IF-MoS_2 which is important for realizing the potential of transition metal dichalcogenides for electronics and solid state lubrication applications.[15,17−24,26] At the same time, this work advances the understanding of novel electronic effects in low-dimensional semiconducting nanomaterials.[27−29]

RESULTS AND DISCUSSION

Enhanced Optical Properties and Reduced Spin–Orbit Coupling in Re:IF-MoS_2. Figure 2 displays the optical properties of 2H- and IF-MoS_2. We attribute the overall lower optical conductivity of IF-MoS_2 compared to that of the bulk sample (Figure 2a) to size effects. Charge mobility is lower in the nanoparticles compared with the layered analogue because carriers must hop between particles rather than move within an extended two-dimensional sheet. To quantify the strength of the various excitations, we calculated the effective number of electrons $n_{eff}(E)$ from the optical conductivity $\sigma_1(E)$ using the partial sum rule: $n_{eff}(E) = \int_{E_1}^{E_2} E\sigma_1(E)/(\pi h^2 \varepsilon_0)\, dE/(2\pi^2\omega_p^2)$,[32] where $\omega_p^2 = (e^2/V_0 m_0 \varepsilon_0)^{1/2}$ is the plasma frequency, e and m_0 are the charge and mass of an electron, ε_0 is the vacuum dielectric constant, V_0 is the unit cell volume, and E_1 and E_2 are the limits of integration. The integral is estimated based on the full range of our measurements (3 meV–6.4 eV). The result is shown in Figure 2b. $n_{eff}(E)$ is almost zero below the 1.9 eV direct gap, which is split by the A and B excitons.[33,34] It rises above 1.9 eV and increases more rapidly at higher energies because the carriers are driven hard enough to complete various charge transfer excitations.[33,34,36] The effective number of electrons in 2H-MoS_2 is larger than that in IF-MoS_2 due to combined size, strain, and localization effects that emanate from the particulate nature of sample. This result is in line with *dc* resistivity trends in 2H- and IF-WS_2.[37] Figure 2(d–f) shows similar data on the Re:IF-MoS_2 nanoparticles at two characteristic doping levels. As expected the optical conductivity of Re:IF-MoS_2 is larger than that of pristine IF-MoS_2, and $n_{eff}(E)$ increases systematically with doping well above the band gap. Re:IF-MoS_2 is an electron-rich system with a partially filled conduction band,[3,4,8] so both trends are straightforward to understand.

Figure 2c shows a close-up view of the A and B excitons in 2H- and IF-MoS_2.[42] These features red shift from 1.861 and 2.048 eV in the bulk to 1.846 and 2.005 eV in the nested nanoparticles. The exciton peak positions are summarized in Table 1 and appear as horizontal dashed lines in Figure 3a,b. The size-induced exciton softening and associated change in spin–orbit splitting correlates well with intralayer structural strains.[31,33,34,36] Moreover, the 0.015 eV shift of exciton A compared to the 0.043 eV shift of exciton B indicates that the latter is more sensitive to confinement and more strongly perturbed by the formation of the IF- structure.[36] From the exciton positions, we can estimate the spin–orbit splitting for both materials. We find Δ = 0.187 and 0.159 eV for 2H- and IF-MoS_2, respectively, in good agreement with prior work.[33,36] The difference indicates that structural strain[31] modifies band curvature at the *K* point—a conclusion based upon the fact that excitons A and B are attributed to $K_4 \rightarrow K_5$ and $K_1 \rightarrow K_5$ optical transitions as diagramed schematically in Figure 1c,d.[33,34] In single layer MoS_2,[38] the exciton red shifts are even larger, and the spin–orbit coupling is even smaller (Table 1). Confinement thus softens exciton positions and reduces spin–orbit coupling.

Burstein–Moss Shift and Carrier Density Effects in the Nanoparticles. Figure 2f displays a close-up view of excitons A and B for Re:IF-MoS_2 compared to the response of the undoped nanoparticles. The exciton energies are also summarized in Table 2. We immediately notice a clear blue shift of the exciton peak positions with doping. Plotting the difference between the exciton position in the substituted sample and that in the pristine nanoparticles with increasing doping level (Figure 3a,b), we extract a systematic shift. As discussed in a following section, this trend can be understood within the framework of the Burstein–Moss model.[1−4,8]

Figure 1a shows the transitions for excition A and B in pristine IF-MoS_2. For n-type doping, the extra carriers occupy the lower conduction band states, which pushes the excitonic transitions to higher energies (Figure 1b). This is the so-called Burstein–Moss effect.

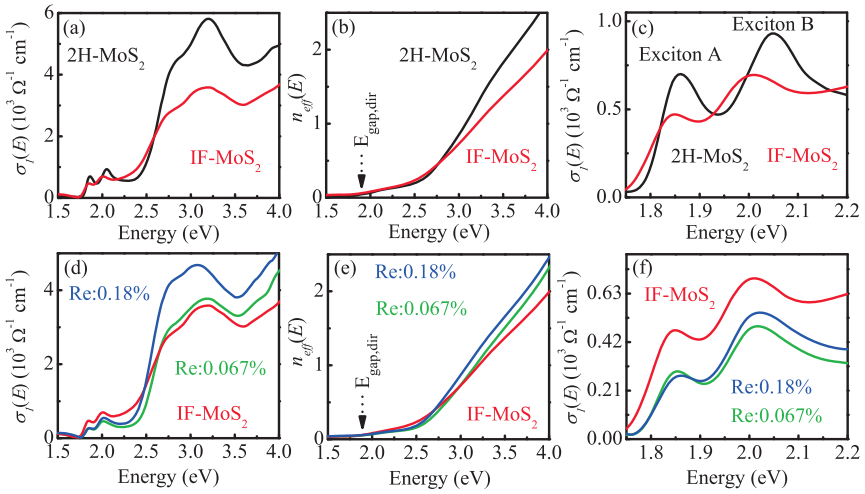

Figure 2. (a,d) 300 K optical conductivity of bulk and nanoscale MoS_2 calculated from a Kramers–Kronig analysis of the measured reflectance. (b,e) Effective number of electrons, $n_{eff}(E)$, as a function of energy. The position of the direct gap is indicated. (c,f) Close-up view of the A and B excitons and their dependence upon size and doping.

TABLE 1. Optical Properties of 2H-, IF-, and Single Layer MoS_2[a]

materials	exciton A (eV)	exciton B (eV)	spin–orbit splitting (eV)	direct gap (eV)
2H-MoS_2	1.861	2.048	0.187	1.903
IF-MoS_2	1.846	2.005	0.159	1.888
single layer MoS_2	1.83[38]	1.98[38]	0.15	1.872

[a] The error bar is ±2 meV on the exciton peak positions. Single sheet data from ref 38 is included for comparison, from which we calculated the spin-orbit splitting and the direct gap.

According to parabolic band theory, the Burstein–Moss shift is given as[8]

$$\Delta E_{BM} = \frac{\hbar^2}{2m^*}(3\pi^2 n)^{2/3} \quad (1)$$

Here, ΔE_{BM} is Burstein–Moss shift, n is carrier density, m^* is the effective electron mass, and $\hbar$ is the reduced Planck constant ($\hbar = h/(2\pi)$). In our case, the carriers are weakly bound rather than free with an estimated activation energy of ~0.19 eV.[20] We also take $m^* = 0.48m_0$, where m_0 is the free electron mass.[43] Figure 3(c,d) shows the predicted Burstein–Moss shift as a function of doping level compared with the measured optical data for Re:IF-MoS_2. Excellent agreement is obtained. The Burstein–Moss shift is observed in a number of traditional semiconductors like CdSe, $In_{0.53}Ga_{0.47}As/InP$, and $CuInSe_2$.[1−4,8] It has also been observed in nanoscale ZnO and InAs.[27−29] To our knowledge, Re:IF-MoS_2 represents the first example of such a mechanism in a nanoscale transition metal dichalcogenide.

Using eq 1 and the experimental results, we can roughly estimate the carrier density. We find n is approximately 9.0×10^{17} cm^{-3} for Exciton A and 2.3×10^{18} cm^{-3} for Exciton B in Re(0.18%):IF-MoS_2. As a consistency check, we can back-calculate the activation energy and compare it to the literature value from ref 20. We begin by estimating the total electron density (ρ_{Tot})

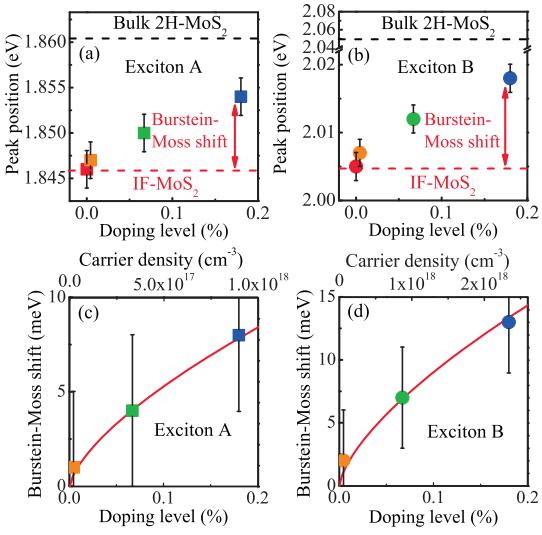

Figure 3. (a,b) A and B exciton energies as a function of Re doping level. Black and red dashed lines indicate 2H- and IF- values, which represent the two limiting cases. (c,d) Burstein–Moss shift as a function of Re doping. Red solid curves denote the predicted shift according to the model discussed in the text. Good agreement between the experimental data and theoretical prediction is observed for both excitons. This agreement establishes a quantitative connection between actual dopant concentration and carrier density. Error bars are ±2 meV on the peak position and ±4 meV on the energy shift. Clustering of the Re centers is anticipated at higher doping levels. This should cause the experiment points to diverge from the Burstein–Moss prediction as dopant centers begin to segregate.[39] The size of the Burstein–Moss shifts will support the understanding of excitonic states by resonance Raman scattering.[40,41].

provided by Re as $\rho_{Tot} = (N \cdot 0.0018/V) = 3.4 \times 10^{19}$ cm^{-3} for Re(0.18%):IF-MoS_2, where N is the number of formula units/unit cell, and V is the volume of the MoS_2 formula unit. We can then express the actual carrier density as $\rho_{Act} = \rho_{Tot} \exp(E_a/(kT))$, where E_a is activation energy, and k is Boltzmann constant.[4] Inserting the aforementioned carrier density for Exciton A of $\rho_{Act} = 9.0 \times 10^{17}$ cm^{-3}, we

TABLE 2. Optical Properties of IF-MoS_2 and the Re-Doped Systems[a]

materials	exciton A (eV)	exciton B (eV)	spin−orbit splitting (eV)	direct gap (eV)	ΔE_{BM} A (meV)	ΔE_{BM} B (meV)
IF-MoS_2	1.846	2.005	0.159	1.888		
Re:IF-MoS_2 (0.0044%)	1.847	2.007	0.160	1.889	1	2
Re:IF-MoS_2 (0.06%)	1.850	2.012	0.162	1.892	4	7
Re:IF-MoS_2 (0.18%)	1.854	2.018	0.164	1.896	8	13

[a] The error bar is ±2 meV on the exciton peak positions. The Burstein−Moss (BM) shift in Re:IF-MoS_2 is calculated based on undoped IF-MoS_2.

estimate an activation energy E_a of about 0.09 eV. The same analysis for Exciton B gives $E_a \approx 0.07$ eV. These values are in reasonable agreement with the density-functional tight-binding result ($E_a = 0.19$ eV),[20] although the error bars are admittedly large.

Band Gap Trends and Structure−Property Relations. 2H-MoS_2 is an indirect band gap material with a $\Gamma \rightarrow {}^1/_2 \approx \Gamma K$ transition of 1.25 ± 0.05 eV.[33,34,44] The intensity of the indirect gap excitation is lower than that of the direct gap, making it difficult to discern—even in measurements on single crystals.[44] While similar indirect band gap structures have been predicted to exist in metal dichalcogenide nanotubes (and presumably the nanoparticles),[45] none have yet been observed by optical means.[36] Our measurements on IF-MoS_2 and the various n-doped materials studied here are similar, though, strictly speaking, an assignment of and correspondingly a distinction between direct and indirect gaps is formally impossible for a nanoparticle. This lack of distinction presents itself as a crossover to direct gap behavior in systems with atomically thin layers.[17] Getting back to IF-MoS_2, our spectra do seem to reveal at least one of the corresponding excitations. Recall that the direct gap in MX_2 materials is split by the A and B excitons.[33,34] We can therefore estimate the direct band gap using exciton A as $E_{g,dir} = E_A + E_{Ryd}$, where $E_{Ryd} = 0.042$ eV is the exciton Rydberg constant.[46] Using this formula, we find that the direct gap of 2H-MoS_2 is 1.903 eV which agrees reasonably well with Beal's result (1.95 eV).[47] Assuming that IF-MoS_2 has the same Rydberg constant, we can extract the gap position as $E_{g,dir} = 1.888$ eV (Table 1). This value is close to that of single-layer MoS_2[35] calculated in the same manner (1.872 eV). We attribute the decrease to strain and confinement effects.[34] We also extended this analysis to include Re doping in the nanoparticles. As shown in Table 2, the gap shifts to higher energy with increased doping. For Re-(0.18%):IF-MoS_2, we find $E_{g,dir} = 1.896$ eV. This trend is a straightforward consequence of the Burstein−Moss effect.[8]

Finally, we compare the size of the Burstein−Moss shift in Re:IF-MoS_2 with that in other n-doped semiconductors. The shift in Re:IF-MoS_2 is significantly smaller than, for instance, $In_{0.53}Ga_{0.47}As$/InP, n-InSb, n- and p-type InAs, and In-doped ZnO.[1,7,8,27] We attribute the reduction of the Burstein−Moss shift in n-doped transition metal dichalcogenides like Re:IF-MoS_2 to the combination of two effects. First, the concentration of Re is very low in the nanoparticles. As indicated in eq 1, shift is directly proportional to carrier density, so low doping levels automatically yield small shifts. Second, finite length scale effects in the nanoparticles modify at least certain aspects of the electronic structure as discussed above—possibly even the activation energy. The 0.07−0.09 eV activation energy estimated from our data is certainly much larger than that in traditional semiconductors.[4] The combination of low doping levels and nonzero activation energy is highly desirable for molecular electronics and solid state lubrication applications.[23] The key to devices is, of course, the ability to control carrier density with both chemical doping and electric field.[24,26]

CONCLUSION

To summarize, we investigated the optical properties of rhenium-doped IF-MoS_2 and compared the results with pristine nanoparticles and the 2H-bulk material. Confinement softens the exciton positions and reduces spin−orbit coupling, whereas doping has the opposite effect. Moreover, the doping-induced blue shift of excitons A and B compares well with predictions from the Burstein−Moss model, establishing a quantitative link between the actual dopant concentration and carrier density. These findings are important for understanding finite length scale and doping effects in transition metal dichalcogenides and the more complicated functional materials that emanate from this parent compound. They also illustrate the utility of reaching beyond traditional bulk semiconductors and quantum dots to explore layered systems like metal dichalcogenides.

MATERIALS AND METHODS

Re:IF-MoS_2 was synthesized by a high temperature (850 °C) gas phase reaction from MoO_3 powder by a three-step procedure in a vertical bed reactor.[21−23,30] The resulting nanoparticles range in size from 50 to 140 nm in diameter, with a mean size of 80 nm. Actual Re concentrations of 0.0044%, 0.067%, and 0.18% were obtained.[22] 2H-MoS_2 (99%) was purchased directly from Alfa Aesar. Near normal reflectance was measured over a wide energy range (3 meV−6.4 eV, 0.1 nm resolution) with a series of

spectrometers,[31] and a 2000 Å aluminum overcoat was used to correct for scattering effects. A Kramers–Kronig analysis was used to obtain the optical constants.[32] Optical conductivity, $\sigma_1(E)$, and sum rules on this quantity are of interest here.

Conflict of Interest: The authors declare no competing financial interest.

Acknowledgment. This research is supported by the U.S. Department of Energy, Office of Basic Energy Sciences, Division of Materials Sciences and Engineering under Award DE-FG02-01ER45885 (J.L.M.) and NanoMaterials, Ltd. (R.T.). R.T. is the director of the Helen and Martin Kimmel Center for Nanoscale Science and holds the Drake Family Chair in Nanotechnology. We thank D. Mazumdar for useful discussions.

REFERENCES AND NOTES

1. Burstein, E. Anomalous Optical Absorption Limit in InSb. *Phys. Rev.* **1954**, *93*, 632–633.
2. Moss, T. S. The Interpretation of the Properties of Indium Antimonide. *Proc. Phys. Soc. B* **1954**, *67*, 775–782.
3. Tenne, R.; Flaisher, H.; Triboulet, R. Photoelectrochemical Etching of ZnSe and Nonuniform Charge Flow in Schottky Barriers. *Phys. Rev. B* **1984**, *29*, 5799–5804.
4. Tenne, R.; Jagerwaldau, R.; Luxsteiner, M.; Bucher, E.; Rioux, J.; Levyclement, C. Transport and Optical Properties of Low-Resistivity CdSe. *Phys. Rev. B* **1990**, *42*, 1763–1772.
5. Lee, J. J.; Yang, C. S.; Park, Y. S.; Kim, K. H.; Kim, W. T. The Burstein–Moss Effect in Cu_2GeSe_3: Co^{2+} Single Crystals. *J. Appl. Phys.* **1999**, *86*, 2914–2916.
6. Wu, J.; Walukiewicz, W.; Shan, W.; Yu, K. M.; Ager, J. W.; Haller, E. E.; Lu, H.; Schaff, W. J. Effects of the Narrow Band Gap on the Properties of InN. *Phys. Rev. B* **2002**, *66*, 201403.
7. Sarkar, A.; Ghosh, S.; Chaudhuri, S.; Pal, A. K. Studies on Electron Transport Properties and the Burstein–Moss Shift in Indium-Doped ZnO Films. *Thin Solid Films* **1991**, *204*, 255–264.
8. Munoz, M.; Pollak, F. H.; Kahn, M.; Ritter, D.; Kronik, L.; Cohen, G. M. Burstein–Moss Shift of n-Doped $In_{0.53}Ga_{0.47}As$/InP. *Phys. Rev. B* **2001**, *63*, 233302.
9. Evans, B. L.; Young, P. A. Optical Absorption and Dispersion in Molybdenum Disulphide. *Proc. R. Soc. London, A* **1965**, *284*, 402–422.
10. Connell, G. A. N.; Wilson, J. A.; Yoffe, A. D. Effects of Pressure and Temperature on Exciton Absorption and Band Structure of Layer Crystals: Molybdenum Disulphide. *J. Phys. Chem. Sol.* **1969**, *30*, 287–296.
11. Tiong, K. K.; Shou, T. S. Anisotropic Electrolyte Electroreflectance Study of Rhenium-Doped MoS_2. *J. Phys.: Condens. Mater.* **2000**, *12*, 5043–5052.
12. Yen, P. C.; Hsu, H. P.; Liu, Y. T.; Huang, Y. S.; Tiong, K. K. Temperature Dependences of Energies and Broadening Parameters of the Band-Edge Excitons of Re-Doped WS_2 and 2H-WS_2 Single Crystals. *J. Phys.: Condens. Matter* **2004**, *16*, 6995–7005.
13. The red shift of exciton A and B compared with that of the undoped sample was attributed to the coexistence of 3R and 2H phases in the sample.[11]
14. Tenne, R. Inorganic Nanotubes and Fullerene-like Nanoparticles. *Nat. Nanotechnol.* **2006**, *1*, 103–111.
15. Radisavljevic, B.; Radenovic, A.; Brivio, J.; Giacometti, V.; Kis, A. Single-Layer MoS_2 Transistors. *Nat. Nanotechnol.* **2011**, *6*, 147–150.
16. Sahoo, J. K.; Tahir, M. N.; Yella, A.; Schladt, T. D.; Pfeiffer, S.; Nakhjavan, B.; Mugnaioli, E.; Kolb, U.; Tremel, W. Self-Assembly of Metal Chalcogenide/Metal Oxide Nanostructures Based on the Degree of Pearson Hardness. *Chem. Mater.* **2011**, *23*, 3534–3539.
17. Wang, Q. H.; Kalantar-Zadeh, Kourosh; Kis, Andras; Coleman, J. N.; Strano, M. S. Electronics and Optoelectronics of Two-Dimensional Transition Metal Dichalcogenides. *Nature Nanotechnol.* **2012**, *7*, 699–712.
18. Ye, J. T.; Zhang, Y. J.; Akashi, R.; Bahramy, M. S.; Arita, R.; Iwasa, Y. Superconducting Dome in a Gate-Tuned Band Insulator. *Science* **2012**, *338*, 1193–1196.
19. Shanmugam, M.; Bansal, T.; Durcan, C. A.; Yu, B. Molybdenum Disulphide/Titanium Dioxide Nanocomposite-Poly 3-Hexylthiophene Bulk Heterojunction Solar Cell. *Appl. Phys. Lett.* **2012**, *100*, 153901.
20. Deepak, F. L.; Popovitz-Biro, R.; Feldman, Y.; Cohen, H.; Enyashin, A.; Seifert, G.; Tenne, R. Fullerene-Like $Mo(W)_{1-x}Re_xS_2$ Nanoparticles. *Chem. Asian J.* **2008**, *3*, 1568–1574.
21. Rosentsveig, R.; Margolin, A.; Gorodnev, A.; Popovitz-Biro, R.; Feldman, Y.; Rapoport, L.; Novema, Y.; Naveh, G.; Tenne, R. Synthesis of Fullerene-like MoS_2 Nanoparticles and Their Tribological Behavior. *J. Mater. Chem.* **2009**, *19*, 4368–4374.
22. Yadgarov, L.; Stroppa, D. G.; Rosentsveig, R.; Ron, R.; Enyashin, A. N.; Houben, L.; Tenne, R. Investigation of Rhenium Doped MoS_2 Nanoparticles with Fullerene-like Structure (IF-MoS_2). *Z. Anog. Alle. Chem.* **2012**, *638*, 2610–2616.
23. Yadgarov, L.; Rosentsveig, R.; Leitus, G.; Albu-Yaron, A.; Moshkovich, A.; Perfilyev, V.; Vasic, R.; Frenkel, A. I.; Enyashin, A. N.; Seifert, G. Controlled Doping of MS_2 (M = W, Mo) Nanotubes and Fullerene-like Nanoparticles. *Angew. Chem., Int. Ed.* **2012**, *51*, 1148–1151.
24. Kou, L.; Tang, C.; Zhang, Y.; Heine, T.; Chen, C.; Frauenheim, T. Tuning Magnetism and Electronic Phase Transitions by Strain and Electric Field in Zigzag MoS_2 Nanoribbons. *J. Phys. Chem. Lett.* **2012**, *3*, 2934–2941.
25. Amasha, S.; Keller, A. J.; Rau, I. G.; Carmi, A.; Katine, J. A.; Shtrikman, H.; Oreg, Y.; Goldhaber-Gordon, D. Pseudospin-Resolved Transport Spectroscopy of the Kondo Effect in a Double Quantum Dot. *Phys. Rev. Lett.* **2013**, *110*, 046604.
26. Popov, I.; Seifert, G.; Tomanek, D. Designing Electrical Contacts to MoS_2 Monolayers: A Computational Study. *Phys. Rev. Lett.* **2012**, *108*, 156802.
27. Mocatta, D.; Cohen, G.; Schattner, J.; Millo, O.; Rabani, E.; Banin, U. Heavily Doped Semiconductor Nanocrystal Quantum Dots. *Science* **2011**, *332*, 77–81.
28. Subramanian, V.; Wolf, E. E.; Kamat, P. V. Green Emission to Probe Photoinduced Charging Events in ZnO–Au Nanoparticles. Charge Distribution and Fermi-level Equilibration. *J. Phys. Chem. B* **2003**, *107*, 7479–7485.
29. Stroyuk, A. L.; Shvalagin, V. V.; Kuchmii, S. Y. Photochemical Synthesis and Optical Properties of Binary and Ternary Metal-Semiconductor Composites Based on Zinc Oxide Nanoparticles. *J. Photochem. Photobiol. A: Chem.* **2005**, *173*, 185–194.
30. Zak, A.; Feldman, Y.; Alperovich, V.; Rosentsveig, R.; Tenne, R. Growth Mechanism of MoS_2 Fullerene-like Nanoparticles by Gas-Phase Synthesis. *J. Am. Chem. Soc.* **2000**, *122*, 11108–11116.
31. Sun, Q. C.; Xu, X. S.; Vergara, L. I.; Rosentsveig, R.; Musfeldt, J. L. Dynamical Charge and Structural Strain in Inorganic Fullerenelike MoS_2 Nanoparticles. *Phys. Rev. B* **2009**, *79*, 205405.
32. Wooten, F. *Optical Properties of Solids*; Academic Press: New York, 1972.
33. Coehoorn, R.; Haas, C.; Degroot, R. A. Electronic Structure of $MoSe_2$, MoS_2, and WSe_2. II. The Nature of the Optical Band Gaps. *Phys. Rev. B* **1987**, *35*, 6203–6206.
34. Boker, T.; Severin, R.; Muller, A.; Janowitz, C.; Manzke, R.; Voss, D.; Kruger, P.; Mazur, A.; Pollmann, J. Band Structure of MoS_2, $MoSe_2$, and α-$MoTe_2$: Angle-Resolved Photoelectron Spectroscopy and *ab Initio* Calculations. *Phys. Rev. B* **2001**, *64*, 235305.
35. Lee, H. S.; Min, S.-W.; Chang, Y.-G.; Park, M. K.; Nam, T.; Kim, H.; Kim, J. H.; Ryu, S.; Im, S. MoS_2 Nanosheet Phototransistors with Thickness-Modulated Optical Energy Gap. *Nano Lett.* **2012**, *12*, 3695–3700.
36. Frey, G. L.; Elani, S.; Homyonfer, M.; Feldman, Y.; Tenne, R. Optical-Absorption Spectra of Inorganic Fullerene-like MS_2 (M = Mo, W). *Phys. Rev. B* **1998**, *57*, 6666–6671.
37. Kopnov, F.; Yoffe, A.; Leitus, G.; Tenne, R. Transport Properties of Fullerene-like WS_2 Nanoparticles. *Phys. Stat. Sol. B* **2006**, *243*, 1229–1240.
38. Splendiani, A.; Sun, L.; Zhang, Y.; Li, T.; Kim, J.; Chim, C.-Y.; Galli, G.; Wang, F. Emerging Photoluminescence in Monolayer MoS_2. *Nano Lett.* **2010**, *10*, 1271–1275.

39. According to XAFS, some segregation is already present at 0.18%,[23] although the optics is not yet sensitive to this fact.
40. Livneh, T.; Sterer, E. Resonant Raman Scattering at Exciton States Tuned by Pressure and Temperature in 2H-MoS_2. *Phys. Rev. B* **2010**, *81*, 195209.
41. Staiger, M.; Rafailov, P.; Gartsman, K.; Telg, H.; Krause, M.; Radovsky, G.; Zak, A.; Thomsen, C. Excitonic Resonances in WS_2 Nanotubes. *Phys. Rev. B* **2012**, *86*, 165423.
42. Higher order excitons are found at low temperature. They also depend on doping in the nanoparticles.
43. Kaasbjerg, K.; Thygesen, K. S.; Jacobsen, K. W. Phonon-Limited Mobility in n-Type Single-Layer MoS_2 from First Principles. *Phys. Rev. B* **2012**, *85*, 115317.
44. Kam, K. K.; Parkinson, B. A. Detailed Photocurrent Spectroscopy of the Semiconducting Group VIB Transition Metal Dichalcogenides. *J. Phys. Chem.* **1982**, *86*, 463–467.
45. Seifert, G.; Terrones, H.; Terrones, M.; Jungnickel, G.; Frauenheim, T. Structure and Electronic Properties of MoS_2 Nanotubes. *Phys. Rev. Lett.* **2000**, *85*, 146.
46. Lee, P. A. *Optical and Electrical Properties*; Springer: Boston, MA, 1976.
47. Beal, A. R.; Hughes, H. P. Kramers-Kronig Analysis of the Reflectivity Spectra of 2H-MoS_2, 2H-$MoSe_2$ and 2H-$MoTe_2$. *J. Phys. C: Solid State Phys.* **1979**, *12*, 881–890.